

CRISPR editing of the GLI1 first intron abrogates GLI1 expression and differentially alters lineage commitment

Yekaterina Galat^{1,2,3} | Haigang Gu¹ | Mariana Perepitchka^{1,2}  | Robert Taylor¹ | Joon Won Yoon¹ | Xenia A. Glukhova³ | Xiao-Nan Li^{2,4} | Igor P. Beletsky³ | David O. Walterhouse^{1,2,4} | Vasiliy Galat^{1,3,4,5,6} | Philip M. Iannaccone^{1,2,4,5}

¹Developmental Biology Program, Stanley Manne Children's Research Institute, Ann & Robert H. Lurie Children's Hospital of Chicago, Chicago, Illinois

²Pediatrics, Ann & Robert H. Lurie Children's Hospital of Chicago, Northwestern University Feinberg School of Medicine, Chicago, Illinois

³Institute of Theoretical and Experimental Biophysics, Russian Academy of Sciences, Pushchino, Russia

⁴Robert H. Lurie Comprehensive Cancer Center, Northwestern University Feinberg School of Medicine, Chicago, Illinois

⁵Pathology, Northwestern University Feinberg School of Medicine, Chicago, Illinois

⁶ARTEC Biotech Inc, Chicago, Illinois

Correspondence

Vasiliy Galat, PhD, Stanley Manne Children's Research Institute, Box 205, 225 East Chicago Avenue, Chicago, IL 60611.

Email: v-galat@northwestern.edu

Philip M. Iannaccone, MD, PhD, Ann & Robert H. Lurie Children's Hospital of Chicago, Box 204, 225 East Chicago Avenue, Chicago, IL 60611.

Email: pmi@northwestern.edu

Present address

Robert Taylor, Athira Pharma, Seattle, WA

Funding information

Eisenberg Foundation for Charities; National Institutes of Health, Grant/Award Number: P01ES010549; NuSeq Core; Center for Genetic Medicine; Northwestern University Feinberg School of Medicine

Abstract

GLI1 is one of three GLI family transcription factors that mediate Sonic Hedgehog signaling, which plays a role in development and cell differentiation. GLI1 forms a positive feedback loop with GLI2 and likely with itself. To determine the impact of GLI1 and its intronic regulatory locus on this transcriptional loop and human stem cell differentiation, we deleted the region containing six GLI binding sites in the human GLI1 intron using CRISPR/Cas9 editing to produce H1 human embryonic stem cell (hESC) GLI1-edited clones. Editing out this intronic region, without removing the entire GLI1 gene, allowed us to study the effects of this highly complex region, which binds transcription factors in a variety of cells. The roles of GLI1 in human ESC differentiation were investigated by comparing RNA sequencing, quantitative-real time PCR (q-rtPCR), and functional assays. Editing this region resulted in GLI1 transcriptional knockdown, delayed neural commitment, and inhibition of endodermal and mesodermal differentiation during spontaneous and directed differentiation experiments. We found a delay in the onset of early osteogenic markers, a reduction in the hematopoietic potential to form granulocyte units, and a decrease in cancer-related gene expression. Furthermore, inhibition of GLI1 via antagonist GANT-61 had similar in vitro effects. These results indicate that the GLI1 intronic region is critical for the feedback loop and that GLI1 has lineage-specific effects on hESC differentiation. Our work is the first study to document the extent of GLI1 abrogation on early stages of human development and to show that GLI1 transcription can be altered in a therapeutically useful way.

KEYWORDS

CRISPR/Cas9, embryonic stem cells, GANT-61, GLI1 first intron, GLI1 oncogene, Sonic Hedgehog pathway

1 | INTRODUCTION

The Sonic Hedgehog (SHH) signal transduction pathway is mediated by GLI1, GLI2, and GLI3 transcription factors and plays several roles

in normal development.¹⁻⁴ Following inhibition of the patched (PTCH) receptor by the SHH ligand, the transmembrane protein smoothened (SMO) releases its inhibition of GLI family transcription factors. GLI1 functions downstream of GLI2 and GLI3 during development,

This is an open access article under the terms of the Creative Commons Attribution-NonCommercial-NoDerivs License, which permits use and distribution in any medium, provided the original work is properly cited, the use is non-commercial and no modifications or adaptations are made.

©2021 The Authors. STEM CELLS published by Wiley Periodicals LLC on behalf of AlphaMed Press 2021

regulating cell proliferation and morphogenesis in many organ systems. In humans, GLI1 inactivation is associated with a phenotypic spectrum extending from isolated postaxial polydactyly to an Ellis-van Creveld syndrome (EVC)-like condition.⁵ Additionally, a significant cancer burden arises with dysregulation of the SHH signal transduction pathway.^{3,6,7} Hedgehog signaling is believed to be active in up to one-third of all human cancers,⁸⁻¹² and GLI1 gene targets sustain proliferation, inhibit apoptosis,¹³ promote angiogenesis,^{14,15} and increase tumor cell migration.¹⁶ Furthermore, GLI1 expression is associated with chemotherapeutic drug resistance.^{17,18}

GLI1 is transcriptionally activated by GLI2.¹⁹⁻²² More specifically, GLI1 is in a positive feedback loop with GLI2¹² and likely with itself because it activates GLI1 reporters.²³ These feedback loops are considered to be an important element that connects GLI1 expression with cancer phenotypes. If constitutively active, they will continue to drive GLI1 expression, enabling GLI1 to assume an oncogenic role. On the other hand, negative regulation of this transcriptional feedback comes from GLI3, translational repression of GLI1, or the long non-coding RNA (lncRNA) GLI1as.

Our sequencing and public reference sequence data provide further insight into the GLI1-GLI2 positive feedback loop by highlighting six GLI binding sites (GBS) in the first intron of the human GLI1 gene. GLI1 and GLI2 bind the six GBS in this region and activate reporter expression. Elimination of some GB sites attenuates transcriptional activation of the transfected reporter construct, and removing the region containing all sites eliminates reporter gene activation. Additionally, this region has an open chromatin configuration and activating histone marks. In aggregate, these findings indicate that the six GBS are active cis elements within a complex enhancer region and could regulate GLI1 expression²³ *in vivo*.

GLI1 is highly expressed in mesenchymal stem cells (MSCs),²⁴ neural stem cells (NSCs),²⁵ and embryonic stem cells (ESCs).²⁶ In MSCs, upregulation of GLI proteins promotes osteogenic differentiation by inhibiting PPAR γ and C/EBP α .²⁴ Overexpression of SHH and/or GLI1 in human ESCs enhances production of neural progenitor and dopaminergic neurons. For example, by binding to Nanog regulatory sequences, GLI1 upregulates Nanog expression, which enhances NSC self-renewal.²⁷ As an added consideration, Po et al show that, even though p53 downregulation activates SHH, p53 is actually not required for SHH control of Nanog. We have also previously shown that p53 effects are mediated in part by competition with GLI1 for the transcriptional coactivator TAF9.²⁸ Following its expression, Nanog then binds GLI proteins in ESCs and represses GLI1-mediated transcriptional activation.

Overall, despite the GLI1 gene's widespread developmental impact, the expression profiles of GLI1 during differentiation and its function in stem cells are not yet clear. Given this context and the important role of GLI1 in cancer, we established a stem cell model to study the underlying connection between the region containing six GBS in the GLI1 first intron, GLI1 expression, and GLI1 function during early stages of ESC development. In the null GLI1 mouse model, GLI2 apparently can compensate, explaining why GLI1 KO animals do not seem to develop an obvious phenotype.²⁹⁻³¹ Editing out the GLI1 intronic region, without removing the entire GLI1 gene, allowed us to investigate the effects of this highly complex region, which binds many transcription factors in a variety of cell types.

Significance statement

Using the CRISPR/Cas9 strategy, a regulatory region of the first intron of the GLI1 gene in a human embryonic stem cell model edited out in this study. This region contains six highly conserved GLI1 binding sites. The editing significantly lowered GLI1 transcription in the heterozygous state and reduced GLI1 expression to barely detectable levels in the homozygous state. Such alteration in GLI1 expression significantly decreased ectodermal, mesodermal, and endodermal marker expression. This resulted in significant differentiation defects: a reduction in blast colonies and hematopoietic potential, a delay in the onset of early osteogenic markers, delayed neural differentiation, and a reduction in cancer-related gene expression.

We hypothesized that the regulatory region containing the six GBS regulates GLI1 expression, which in turn affects ESC differentiation. To gain insight into the developmental roles of this regulatory region, a combination of spontaneous differentiation in embryoid bodies, directed differentiation, small molecule inhibitors, and RNA sequencing (RNA-Seq) were used. We extend the observation that GLI1 and GLI2 transcription factors bind the six GBS in the GLI1 first intron, thereby activating GLI1 transcription. *In vivo* CRISPR/Cas9 editing enabled us to reduce GLI1 expression to barely detectable levels, which significantly affected GLI1 target genes and resulted in lineage-specific effects on differentiation. In light of this, abrogation of GLI1 expression makes the region and the protein complexes that occupy it attractive therapeutic targets, particularly in cancer.

2 | MATERIALS AND METHODS

2.1 | Cell line

H1 (WA01), a well-characterized human embryonic stem cell (hESC) line,³² was purchased from WiCell (Madison, Wisconsin; <https://www.wicell.org/home/stem-cells/catalog-of-stem-cell-lines/wa01.cmsx>). The cells were maintained on Matrigel-coated culture dishes in mTeSR1 medium (STEMCELL Technologies) or StemMACS iPS-Brew XF (Miltenyi Biotec).

2.2 | Generation of CRISPR plasmids

Single guide (sgRNA) upstream and downstream sequences of the six GBS were designed using Optimized CRISPR Design (Dr. Feng Zhang's Lab in Massachusetts Institute of Technology; <http://crispr.mit.edu/>) and Cas-Designer (Dr. Jin-Soo Kim's Lab in Seoul National University; <http://www.rgenome.net/cas-designer/>). The oligos were annealed and cloned into px330 vector (Addgene, Plasmid #42230).

The upstream and downstream homolog arms were amplified by PCR with Q5 High-Fidelity DNA Polymerase (M0491S, New England Biolab [NEB], Massachusetts) and cloned into HR700PA-1 Gene Knock-out Targeting Vector (System Biosciences [SBI], California) with NEBuilder HiFi DNA Assembly Master Mix (E2621S, NEB). The sequences were verified by Sanger sequencing (GENEWIZ, New Jersey). To generate Targeting Vector carrying Blasticidin, the Puromycin resistance gene was replaced with Blasticidin gBlocks Gene Fragment.

2.3 | Generation of edited H1 ESCs

A total amount of 2 μ g DNA was used for the transfection. Plasmids were cotransfected into H1 hESCs with the Human Stem Cell Nucleofector Kit 1 (VAPH-5012, Lonza) in a Nucleofector 2b device. H1 hESCs were cultured and the potentially positive clones were collected. After 72 hours, 500 ng/mL Puromycin dihydrochloride (NA0310, Sigma) was added to the culture media. Genomic DNA of transfected H1 hESCs was isolated with PureLink Genomic DNA Kits. Genotyping of transfected H1 hESC clones was performed with DreamTaq Green PCR Master Mix according to the manufacturer's protocol. To generate homozygous-edited H1 hESCs, a targeting vector carrying Blasticidin was cotransfected with a px330 vector carrying sgRNA by using the Nucleofector 2b device. After 72 hours, 5 μ g/mL Blasticidin S HCL (Thermo Fisher Scientific) and 500 ng/mL Puromycin dihydrochloride were used to select the double-edited clones.

2.4 | GLI1 Western blot analysis

The following procedures were carried out at 4°C. Approximately 1×10^6 cells were resuspended and incubated in 0.15 mL of RIPA buffer (Sigma) and protease inhibitor cocktail (Pierce) for 5 minutes with rocking. The protein concentration was determined with BCA assay kit (Pierce). All the following procedures were carried out at room temperature. The GLI1 protein was separated on SDS-PAGE gels, transferred onto a nitrocellulose membrane, and incubated in PBST buffer with 5% milk for 30 minutes. The membrane was washed with PBST buffer, incubated with polyclonal rabbit GLI1 antibody (Cell Signaling Technology; cat. no. 2354) (1:15 000 dilution) in PBST buffer with 5% milk for overnight at 4°C. The membranes were washed with PBST buffer (1X PBS, 0.3% Tween-20) and incubated with secondary antibody conjugated with HRP (Donkey anti Rabbit IgG-HRP, Santa Cruz Biotech; cat. no. sc-2077) for 1 hour (1:15 000 dilution in PBST with 5% milk). The membrane was then washed 3x with PBST buffer. The GLI1 protein was visualized using SuperSignal West Femto chemiluminescence kit (Thermo Fisher Scientific). For GAPDH Western blot analysis, the same membrane was stripped with stripping buffer (Thermo Fisher) for 30 minutes at room temperature and then incubated in PBST buffer with 5% milk for 30 minutes. The membrane was washed with PBST buffer and incubated with polyclonal rabbit GAPDH antibody (Cell Signaling Technology; cat. no.14C10) (1:30 000 dilution) in PBST buffer with 5% milk for 1 hour at room temperature. The membranes were

then washed with PBST buffer and incubated with secondary antibody conjugated with HRP (Donkey anti Rabbit IgG-HRP, Santa Cruz Biotech; cat. no. sc-2077) for 1 hour (1:30 000 dilution in PBST with 5% milk) at room temperature. The membrane was then washed 3x with PBST buffer. The GAPDH protein was visualized using SuperSignal West Pico chemiluminescence kit (Thermo Fisher Scientific).

2.5 | Spontaneous differentiation

Single cells were plated onto nonattachment plates and maintained in ESC media without FGF- β in the presence of fetal bovine serum (FBS).

2.6 | Spontaneous differentiation in the presence of GANT-61

Wild-type (WT) H1 hESC single cells were plated onto nonattachment plates and maintained in ESC media without FGF- β in the presence of FBS. The experimental group was cultured in the presence of GANT-61 (Tocris Biosciences, cat. no. 3191) at a concentration of 5 μ M. The control group was cultured in the presence of 5 μ M DMSO. Media containing GANT-61 was replaced every other day. Embryoid bodies were collected at days 10 and 20. Markers for the three embryologic lineages were analyzed by real-time PCR.

2.7 | Endodermal differentiation

Endodermal differentiation was achieved essentially as described in Reference 33. An amount of 1×10^6 pluripotent stem cells were plated on 60 mm Matrigel coated plates in advanced DMEM/12 medium supplemented with 3 μ M CHIR99021 (STEMCELL Technologies). Differentiation medium was changed every day. The cells were collected at days 3 and 5 of differentiation.

2.8 | Endothelial differentiation

Endothelial differentiation was established by a monolayer induction protocol. Briefly, as described in Reference 34, single cells were plated on 60 mm culture dishes coated with matrigel and cultured overnight in StemMACS iPS-Brew XF (Miltenyi Biotec). Differentiation was induced with media containing advanced DMEM/12 (Life Technologies), glutamax (2.5 mM), ascorbic acid (60 μ g/mL), and CHIR990921 (6 μ M) added on day 0. On day 2 of induction, CHIR990921 was removed from the media. The cells were collected on day 5 of differentiation.

2.9 | Hematopoietic colony forming assay

The hematopoietic colony forming assay was performed in MethoCult H4435 medium (STEMCELL Technologies) supplemented with Flt-3L

(50 ng/mL), IL-7 (20 ng/mL), IL-3 (5 ng/mL), SCF (50 ng/mL), and TPO (40 ng/mL) (PeproTech). After initial coculture with OP9 mouse stromal cells as described in Reference 35, hematopoietic progenitors were isolated on day 8 of differentiation and plated at a density of 1×10^5 cells per 35 mm dish. The colonies were evaluated after 16 days in culture.

2.10 | Blast colony forming assay

The blast colony assay was performed in MethoCult H4100 media mixed with SFEM (STEMCELL Technologies) and supplemented with Heparin, LiCl, Glutamax MTG, Ascorbic Acid (all from Sigma-Aldrich), ExCyte (Millipore), FGF2, VEGF (PeproTech), and BIT 9500 Serum Substitute (STEMCELL Technologies).

2.11 | Neural differentiation

Neural differentiation was performed using the PSC Neural Induction Medium (Thermo Fisher Scientific) according to manufacturer's instructions. Neural progenitor cells NPC(s) were collected at day 7 (early neural) and at day 21 (late neural) for differentiation analysis.

2.12 | Osteogenic differentiation

Osteogenic differentiation was initiated using the MSCgo Osteogenic Differentiation Medium (Biological Industries) according to the manufacturer's instructions.

2.13 | Mineralization assay

Matrix mineralization was quantified using alizarin red staining essentially as in Reference 36. After 3 minutes, cells were thoroughly washed and then destained with cetylpyridinium chloride. Absorbance of the destain solution was quantified using a CIARIOstar plate reader at A_{538nm} (BMG Labtech).

2.14 | MTS assay

MTS cell viability assay was performed using the CellTiter 96Aqueous MTS (Promega, Madison, Wisconsin). Live cells were incubated in DMEM containing 10% FBS, without phenol red, in the presence of MTS reagent for 1 hour. Absorbance was quantified using a CIARIOstar plate reader at MTS_{490nm} (BMG Labtech).

2.15 | Flow cytometry analysis

Cells were harvested with StemPro Accutase (Thermo Fisher Scientific), washed with ice-cold FACS buffer (PBS + 1% FBS + 2 mM

EDTA), and incubated with conjugated antibodies CD31 PE, CD34 FITC, VE-Cadherin APC (Miltenyi Biotech) for 30 minutes at 4°C. Following this, cells were washed with a 0.5% BSA/PBS solution. Data collection was performed via the FACSCalibur (BD Biosciences) and analyzed with FlowJo software (version 10.5.3).

2.16 | Immunohistochemistry

The following procedures were performed at room temperature. Neural cells were fixed with 3.2% paraformaldehyde for 30 minutes and permeabilized for 5 minutes with 0.1% Triton-x-100 in PBS. Cells were then treated with Dako Protein Block for 25 minutes to prevent nonspecific antibody binding. Following this, neural cells were incubated with MAP2 (Santa Cruz, cat. no. SC-74421) and GFAP (Sigma, cat. no. G3893) mouse anti-human, primary antibodies. After washing the cells 3x with Dako Washing Buffer (WB), appropriate Alexa Fluor-conjugated secondary antibodies (Invitrogen) were added to cell culture wells; incubation time was 45 minutes. All antibody dilutions were performed according to manufacturers' instructions. Samples were then washed once more with WB and incubated with DAPI (Sigma Aldrich) for 3 minutes. The immunofluorescent cells were visualized with Leica DM IRB inverted microscope system (Leica, Germany) equipped with the Retiga 4000R camera (QImaging, Canada), which was controlled with Openlab software version 5.0.2 (Perkin-Elmer).

2.17 | RNA isolation

Total RNA was extracted with the RNeasy Mini Kit (Qiagen) via the instructions provided in the manufacturer's protocol. RNA quality and concentration were assessed with a Nanodrop instrument.

2.18 | RNA sequencing analysis

Aliquots of RNA were submitted to Northwestern University's NUSeq Core. The mRNA library was prepared and the samples were analyzed using HiSeq 4000 Sequencing 50 bp, Single Reads. The list of differentially expressed genes was further analyzed using MetaCore and R Studio software (gplots and EnhancedVolcano packages).

2.19 | Quantitative real-time PCR

High-Capacity RNA-to-cDNA kit (Applied Biosystems) was used to reverse transcribe the isolated RNA. Each reaction tube included up to 2 μ g of RNA. The reverse transcription reaction was performed according to manufacturer's instructions via the MBS Satellite (0.2G) Thermal Cycler (Thermo Fisher Scientific). The q-rtPCR reaction mix was prepared by adding 12 ng of cDNA from each sample to the PowerUp SYBR Green Master Mix (2X) (Applied Biosystems). qPCR

was performed (Standard Cycling Mode, primer $T_m < 60^\circ\text{C}$) via the 7500 Fast Real-Time PCR system (Applied Biosystems). The 7500 v2.3 software was used for data collection and gene expression comparisons ($2^{-\Delta\Delta\text{CT}}$ method). Primer sequences provided in Table S2.

2.20 | Small interfering RNA (siRNA) treatment and hematopoietic colony forming assay

Three days prior to CHIR99021 induction, H1 hESCs were plated onto a six-well plate and transfected with two siRNA constructs (4 μg each; obtained from Dr Beletsky) using Lipofectamine 3000 (Invitrogen, Thermo Fisher Scientific, Waltham, Massachusetts) according to the manufacturer's instructions. Briefly, prior to treatment, Lipofectamine 3000 siRNA complexes were prepared in reduced serum medium, OptiMEM (Invitrogen, Thermo Fisher Scientific) at the recommended ratio. Cells were then treated overnight in iPS-Brew Medium (Mltyei Biotech, California). To maintain the desired effect of GLI1 downregulation during differentiation, the cells were transfected a second time 1 day prior to CHIR99021 treatment. The differentiation was then performed as in Section 2.8, followed by Section 2.9. Scrambled siRNA construct (obtained from Dr Beletsky) was used as a control.

3 | RESULTS

3.1 | Clone selection and characterization

Previously, we have shown that the first intron of the GLI1 gene has characteristics of an enhancer and contains six conserved GB sites that bind GLI1 and GLI2.²³ Furthermore, in addition to GLI1, GLI1-AT (GLI1 with a deletion removing the N-terminal repressor domain) and tGLI1 (an isoform of GLI1 present in tumors) also activate gene expression (Figures S1 and S2). Moreover, there are no interactive effects of GLI1 or GLI2 on activation of gene expression (Figures S2 and S3).

To determine the impact of this region on GLI1 expression in stem cells and stem cell differentiation, we deleted the region including the six GBS in the first intron of the GLI1 gene using the CRISPR/Cas9 system (Figure 1A). To increase selection specificity and to delete both alleles, two rounds of editing were performed using two different resistance markers. The final clones were picked manually based on their GFP expression (Figure 1B).

To validate successful CRISPR/Cas9 DNA modification, the isolated clones were genotyped (Figure 1C) and sequenced (Table S1). Reduction of GLI1 expression was confirmed by Western blot analysis (Figure 1D). Compared to wild type clones, quantitative real-time PCR demonstrated that there was up to 50% reduction in GLI1 RNA in the heterozygous clone (#6) and barely detectable levels of GLI1 RNA in the homozygous clone (#65). Furthermore, our results showed a significant decrease in the expression of the GLI1 target PTCH1 in both heterozygous and homozygous clones (Figure 1E). On the other hand,

the deletion of this region had minimal effects on the expression of pluripotent markers OCT4, SOX2, and NANOG (Figure 1F). These results indicate that GBS deletion in the first intron of the GLI1 gene dramatically reduces GLI1 expression in stem cells, without affecting their pluripotency.

3.2 | Spontaneous differentiation

To examine the cellular effects of the GLI1 GBS region deletion, we conducted spontaneous differentiation of heterozygous and homozygous clones (exhibiting most significant downregulation of GLI1) and wild-type pluripotent cells using the embryoid body method. Single cells were plated onto nonattachment plates and maintained in ESC media without FGF- β in the presence of FBS. On day 10 of differentiation, embryoid bodies were collected and early markers of the three embryonic lineages were assessed by real-time PCR. Our results showed that, during spontaneous differentiation, the homozygous-edited clone (#65) retained pluripotency markers at a higher level than the heterozygous clone (#6) or the WT H1 hESC control (Figure 1G), indicating that the edited cells were held in a pluripotent state. The clones also exhibited decreased expression of GLI1 (Figure 1H) and its targets (Figure 1I). Additionally, compared to the WT H1 hESC differentiated control, ectodermal PAX6 and OTX2 (Figure 1J), mesodermal BRACHYURY and PDGFR α (Figure 1K), and endodermal GATA4 and GATA6 (Figure 1L) were significantly downregulated for both heterozygous and homozygous GLI1-edited clones. These data suggest that the deletion of the region containing the GBS significantly affects stem cell differentiation toward all three embryonic lineages, and this effect is most pronounced in the homozygous state. Furthermore, GLI2 expression remained consistent both during spontaneous differentiation (Figure 1H) and directed differentiation (Figure S4). In this case, unlike that of the null GLI1 mouse model, GLI2 does not compensate for GLI1 after the six GBS are deleted.

3.3 | Directed differentiation

To more precisely define the effect of GBS deletion on each lineage, we conducted directed differentiation experiments. The aim was to determine whether early differentiation marker downregulation, observed during spontaneous differentiation, was due to delayed/inhibited differentiation potential or because the edited cells were differentiating faster than control WT H1 hESCs. Furthermore, we also wanted to verify that the significant gene downregulation was due to GLI1 editing rather than nonspecific 3D interactions within the embryoid body differentiation system. The differentiated cells were assessed using functional assays and analyzed using RNA-Seq, real-time PCR, fluorescence-activated cell sorting analysis, and immunofluorescence (IF). For directed differentiation experiments, we chose the homozygous GLI1-edited clone with the most downregulated GLI1 expression (#65). Experiments performed with clone #65 showed that GLI1 downregulation had the most significant effect on mesodermal

differentiation, specifically hematopoietic lineages. To confirm these results, we repeated the experiments using homozygous clone #58 and performed siRNA treatments. Furthermore, to ensure that our data is specific to homozygous GLI1 downregulation, we performed directed differentiation toward hematopoietic lineages using heterozygous clone #6.

3.3.1 | Early mesodermal potential of the GLI1 edited clone

To detect early phenotypic differences in mesodermal differentiation between heterozygous clone #6, homozygous GLI1-edited clone #65, and WT H1 hESCs, we induced differentiation by coculturing

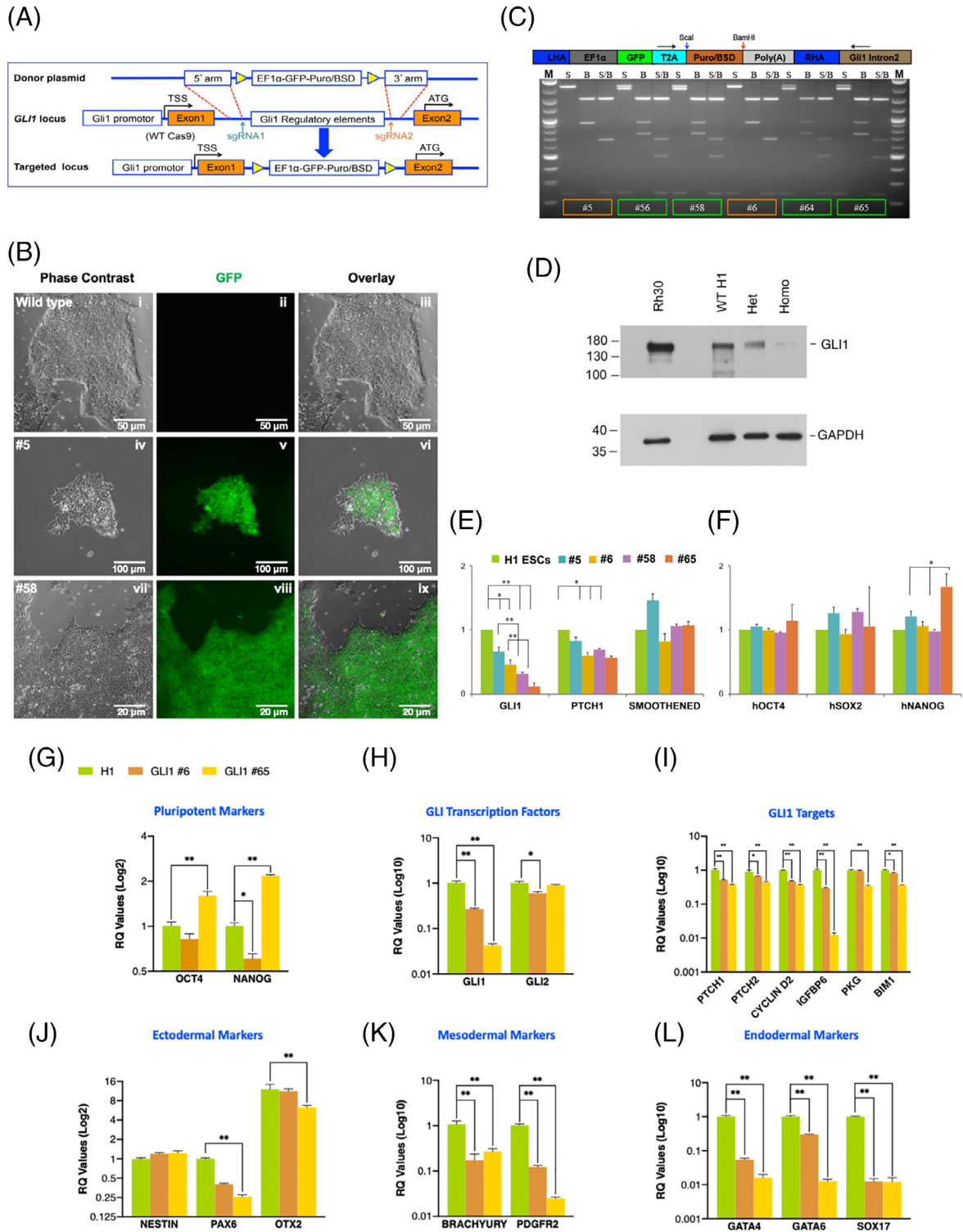


FIGURE 1 Legend on next page.

pluripotent cells with OP9 mouse stromal cells. On day 3 of coculture, the colonies were separated into single cells and placed in semisolid media. After 16 days in culture, the resulting mesenchymal (MS) and Blast (BL) colonies—precursors of primitive blood and endothelial cells—were counted by two individuals and the mean number of colonies was determined (Figure 2A).

We found that an approximately equal number of MS and BL colonies developed in the WT H1 hESCs. There was no significant difference between the number of colonies generated by WT H1 hESC and the heterozygous GLI1-edited clone #6. On the other hand, the homozygous GLI1-edited cells generated significantly more MS colonies than the heterozygous GLI1-edited clone #6 and the WT H1 hESCs (Figure 2B). These data indicate that homozygous deletion of the six GBS of GLI1 skews early stage mesodermal commitment toward the mesenchymal component and results in a smaller number of BL colonies, indicating less prevalence for primitive blood and endothelial cells.

3.3.2 | Endothelial differentiation of GLI1 edited clones (mesodermal lineage)

To further evaluate the effects of GLI1 downregulation on endothelial cell formation, we performed endothelial differentiation, as previously described.³⁷ We used heterozygous GLI1-edited clone #6 and two homozygous GLI1-edited clones #65 and #58 for this experiment. We found that on day 5 of differentiation, the number of CD31+CD34+ endothelial progenitor cells were slightly reduced in the heterozygous GLI1-edited clone #6 compared to WT H1 hESCs. In contrast, the number of CD31+CD34+ endothelial progenitor cells in the homozygous GLI1-edited clones #65 and #58 was significantly reduced and were on average four times smaller compared to WT H1 hESCs (Figure 2C,D). This showed that GLI1 downregulation significantly inhibits endothelial development. Moreover, assessment of cell viability using 7-AAD dye showed that the percentage of live cells in WT and GLI1-edited differentiating cultures was very high, on average 92% to 97% (Figure 2E). There was no significant difference between the numbers of 7-AAD positive cells (Figure 2F), suggesting that the

low efficiency of endothelial differentiation was due to differentiation inhibition, rather than poor cell survival.

Analysis of RNA-Seq data, collected on day 5 of endothelial differentiation, confirmed these results. Using the volcano plot generated by R-Studio software (Figure 2G), we selected differentially expressed vascular and endothelial-related genes with the lowest *P* value and highest fold change (FC). Our selected gene set incorporated genes involved in promoting vascular homeostasis by regulating cell proliferation, migration, adhesion, actin cytoskeletal reorganization, and anti-inflammatory mechanisms in vascular tissue. In comparison to control WT H1 hESCs, this gene set was significantly downregulated in the GLI1-edited cells: CD34 (*P* value = 3.22×10^{-249} , FC = -2.32), THBD (7.90×10^{-5} , -0.97), VWF (1.73×10^{-70} , -2.32), TIE1 (5.15×10^{-51} , -2.72), TEK (2.37×10^{-123} , -1.92), ETS1 (5.62×10^{-113} , -1.19), FLT4 (1.62×10^{-4} , -0.91), KDR (2.29×10^{-30} , -1.23), NOTCH1 (8.85×10^{-4} , -0.63), TAL1 (2.78×10^{-30} , -1.53), and COL22A1 (4.83×10^{-82} , -1.05). Furthermore, the data showed significant downregulation in the RUNX1 gene (2.68×10^{-58} , -3.08), indicating decreased hemogenic potential of derived endothelium in GLI1-edited cells (Figure 2H). To complement these results, pathway analysis revealed significant inhibition of differentiation toward lymphatic, venous, and arterial endothelium as indicated by significant downregulation in SOX18 (3.12×10^{-10} , -1.39), PROX1 (1.73×10^{-70} , -2.32), VEGFR-3 (9.16×10^{-4} , -0.91), HEY1 (3.12×10^{-10} , -0.66), and HEY2 (1.00×10^{-50} , -1.85) (Figure S5).

Additionally, we observed that several genes implicated in various forms of cancer were significantly downregulated in the GLI1-edited cells during vascular formation. For example, the LAPTM4B (*P* value = 1.13×10^{-75} , -0.99) gene is related to metabolic stress tolerance in cancer cells.³⁸ ETS1 (5.62×10^{-113} , -1.19) and FLI1 (5.37×10^{-95} , -1.86) are transcription factors associated with GLI1 upregulation in Ewing sarcoma through the EWSR1/FLI1 translocation fusion protein.³⁹ FLI1 upregulation is also associated with susceptibility to follicular non-Hodgkin lymphoma. Another gene, ADAMTSL1 (4.17×10^{-50} , -3.32), has been associated with chondrosarcoma. ADAMTSL1 may play an important role in cell survival and its downregulation has been linked to significant antitumor

FIGURE 1 Generation and characterization of GLI1-edited H1 hESCs. A, Schematic depiction of the strategy to target the region including the six GBS. Yellow triangles represent LoxP sites. B, (i-ix) Both the heterozygous (#5) and homozygous (#58) clones express green fluorescent protein (GFP) and have similar morphology as wild-type hESCs. C, Genotyping of heterozygous (#5, #6) and homozygous (#56, #58, #64, #65) H1 hESC clones by PCR-RFLP. Black arrows, PCR primers; B, BamHI; BSD, Blasticidin; Puro, Puromycin; S, Scal. D, Western blot analysis showed decreased expression of GLI1 in heterozygous clone #6 (Het) and a dramatic reduction of GLI1 expression in homozygous clone #65 (Homo). Rh30 cells (human rhabdomyosarcoma cells) were used as a positive control for GLI1 protein. E, Real-time PCR analysis showing that the deletion of this region of the GLI1 gene in hESCs dramatically reduced the expression of GLI1 and its target PTCH1. F, Deletion of this region has minimal effects on the expression of pluripotency markers OCT4, SOX2, and NANOG. G, Real-time PCR analysis showing that the GLI1-edited homozygous cells maintain higher pluripotency marker expression, determined in embryoid bodies after 10 days of spontaneous differentiation. H, Real-time PCR analysis showing that the deletion of this region of GLI1 in hESCs maintains reduction in GLI1 expression, but not GLI2, determined under same conditions as in (G). I, Real-time PCR analysis showing that the deletion of this region of the GLI1 gene in hESCs maintains reduction in expression of GLI1 targets, determined under same conditions as in (G). J-L, Real-time PCR analysis showing that the deletion of this region of the GLI1 gene in hESCs significantly reduces the expression of markers associated with ectodermal (J), mesodermal (K), and endodermal (L) lineages (**P* < .05, ***P* < .01). The real-time PCR charts include data presented as mean ± SEM from at least three independent experiments. GBS, GLI binding sites; hESCs, human embryonic stem cells

effects.⁴⁰ TM4SF1 (2.30×10^{-41} , -2.53) is highly expressed in various carcinomas. JAG2 (4.15×10^{-71} , -2.08) was found to be overexpressed in multiple myeloma, but not in nonmalignant plasma cells from tonsils

or bone marrow from healthy individuals or patients with other malignancies⁴¹ (Figure 2). Overall, these findings suggest that the possible role of such genes in these cancers is related to tumor angiogenesis.

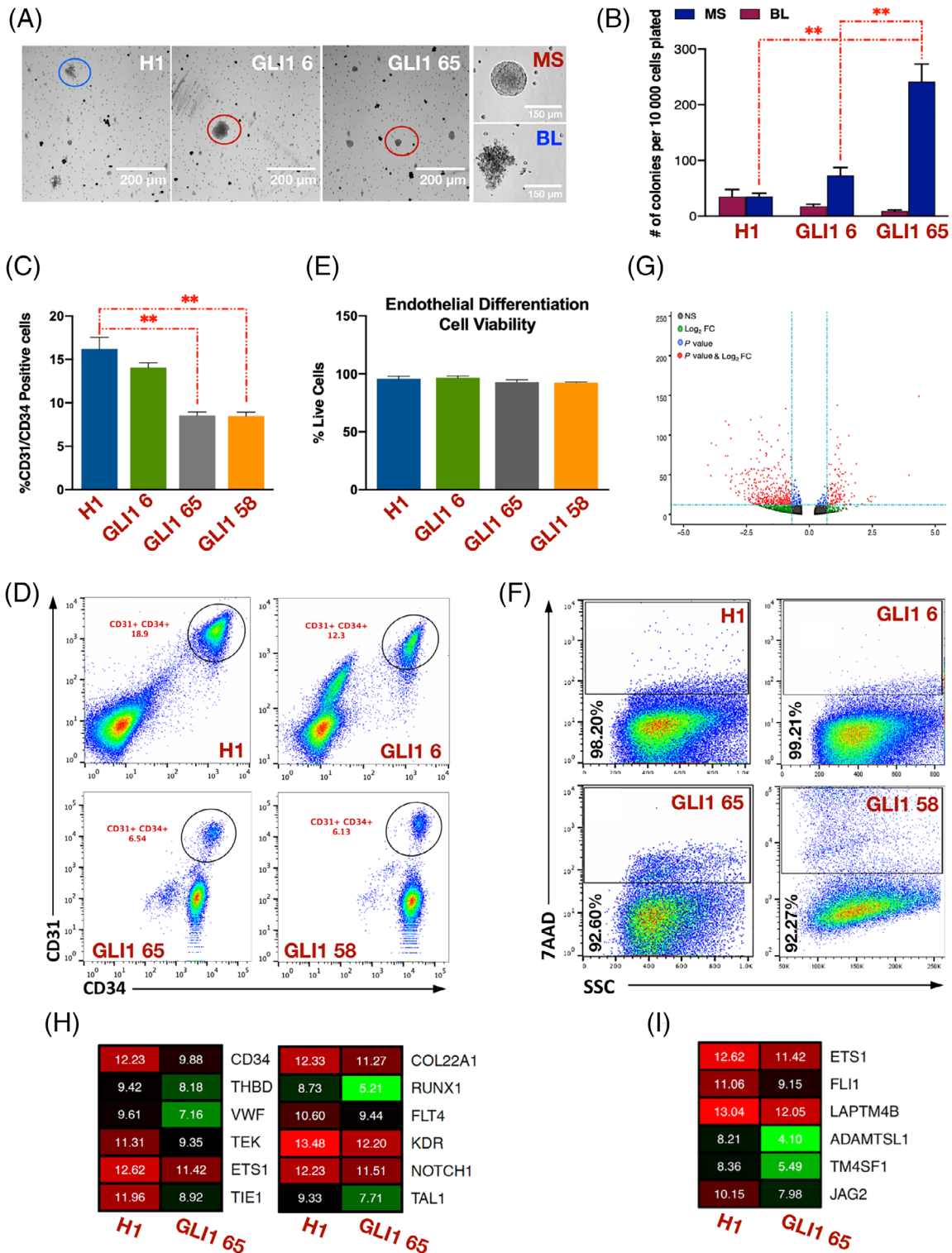


FIGURE 2 Legend on next page.

3.3.3 | Hematopoietic potential

GLI1 downregulation has been shown to affect differentiation and proliferation of myeloid progenitors in mice.⁴² To assess the hematopoietic potential of heterozygous GLI1-edited clone #6 and the homozygous GLI1-edited clone #65, we briefly cocultured the cells isolated on day 5 of endothelial differentiation with OP9 mouse stroma. Hematopoietic progenitors were then placed into semisolid media containing hematopoietic cytokines. After 18 days, the colonies were counted and the numbers were compared to WT H1 hESCs (Figure 3A). We observed no significant difference in the number of granulocyte forming units (CFU-G) between WT H1 hESCs and heterozygous GLI1-edited clone #6. In contrast, the difference in the number of CFU-G between WT H1 hESCs and homozygous GLI1-edited clone #65 was significant. The WT H1 CFU-G count was on average 9× greater than the edited GLI1 clone CFU-G count (Figure 3B).

To confirm that the observed result was due to GLI1 downregulation, we treated WT H1 hESCs with a combination of two siRNAs. GLI1 downregulation was confirmed using Western blot (Figure S5). We found that scrambled RNA-treated progenitors, on average, formed 12.5× greater CFU-G (Figure 3C) and those colonies were also marginally smaller in size (Figure 3D).

3.3.4 | Osteogenic differentiation

GLI1 has been implicated in SHH-mediated specification of the osteoblast lineage.⁴³ Previous work established that GLI1-expressing mesenchymal progenitor cells are responsible for bone formation and fracture repair in mice.⁴⁴ We evaluated the differentiation potential of our MSCs differentiated from WT H1 hESCs and homozygous GLI1-edited cells. Mesenchymal differentiation was established by isolation of a multipotential progenitor at the mesenchymoangioblast stage, as described previously.⁴⁵

Our time point, real-time PCR analysis of osteogenic differentiation showed that ALPL, an early marker of osteogenic differentiation, increased significantly in WT H1 hESCs by day 3. Whereas in the homozygous GLI1 edited cells, the significant increase occurred between day 3 and 6. By day 6, there was no significant difference in

ALPL gene expression between homozygous cells and WT control. Our real-time PCR results also showed no significant difference between the expression of other osteogenic markers, including RUNX2 and BGLAP (Figure 4A). These results suggest that the loss of GLI1 may delay the initiation of bone development.

Evaluation of osteogenic differentiation efficiency using Alizarin Red staining complements our real-time PCR data. On day 8, the results demonstrated that WT H1 hESCs had a significantly greater amount of calcium deposition. By day 10 of differentiation, both WT H1 hESCs and homozygous GLI1-edited cells were highly mineralized (Figure 4B,C). There was no significant difference between absorbance values at 538 nm.

As an added layer of confirmation, the MTS viability assay revealed that the initiation of osteogenic differentiation greatly affected the viability of the GLI1-edited homozygous clones. On day 8 of differentiation, the homozygous clone had five times fewer proliferating cells than WT H1 hESCs. The difference became insignificant as differentiation progressed and the number of viable cells decreased in WT control (Figure 4D). This proliferative profile is reflected in SHH pathway signaling, which promotes osteogenic induction. In comparison to WT H1 hESCs, the GLI1-edited cells had upregulated expression levels of the transcription factor PPAR-gamma (PPARG, P value = 2.20×10^{-37} , FC = 1.94), which inhibits the transcription factor RUNX2 (8.73×10^{-11} , -0.55). Downregulated RUNX2 expression cannot effectively upregulate key osteogenesis-promoting genes such as ALPL (3.78×10^{-15} , -2.99) and COL1A1 (1.77×10^{-5} , -0.18) (Figure S6).

Furthermore, additional pathway analysis and the volcano plot (Figure 4E) showed an even larger array of genes that were differentially expressed with high significance. In addition to PPARG, RUNX2, ALPL, and COL1A1, we expanded our osteogenic gene list to include: BAP1 (P value = .01, FC = -0.19), IGFBP3 (0, -5.86), and SPARC (1.30×10^{-47} , -0.64). These genes were significantly downregulated in the GLI1-edited homozygous cells (Figure 4F).

3.3.5 | Endodermal potential (endodermal lineage)

Endodermal differentiation was achieved using a monolayer differentiation system, as previously described with addition of CHIR99021

FIGURE 2 Assessment of the effect of GLI1 editing on endothelial (mesodermal) differentiation potential of hESCs. A, (Left panel) Representative phase contrast images showing mesangioblast and mesenchymal colonies growing in semisolid media generated from WT H1 hESCs (blue circle) and GLI1-edited clones (#6, #65) (red circles). (Right panel) Higher magnification of mesangioblast (BL) and mesenchymal (MS) colonies. B, A graph showing a significant increase in the number of MS colonies in the GLI1-edited clone #65 (homozygous), but no significant increase in the number of MS colonies in GLI1-edited clone #6 (heterozygous) compared to the WT H1 hESCs during the early mesodermal specification; Bars represent mean \pm SEM from three independent experiments (** P < .001). C,D, A graph and representative flow cytometry analysis showing that the endothelial differentiation efficiency of homozygous GLI1-edited clones is significantly lower than the WT H1 hESCs. Bars represent mean \pm SEM from three independent experiments. E,F, Representative flow cytometry analysis and a graph demonstrating high cell survival during endothelial differentiation. There was no significant difference in survival between the WT H1 hESCs and GLI1-edited clones. G, Volcano plot showing the RNA-Seq data distribution for endothelial differentiation of WT H1 hESCs vs GLI1-edited cells. In relation to WT H1 hESCs, the downregulated genes are on the left and upregulated genes are on the right. H, Heatmap showing vascular-related gene expression comparison between WT H1 hESCs and GLI1-edited clone (#65). The expression, P value, and fold change data for all gene tables were obtained from RNA-Seq analysis. I, Heatmap showing cancer-related gene expression comparison between WT H1 hESC and GLI1-edited cells (#65). hESCs, human embryonic stem cells; RNA-Seq, RNA sequencing; WT, wild-type

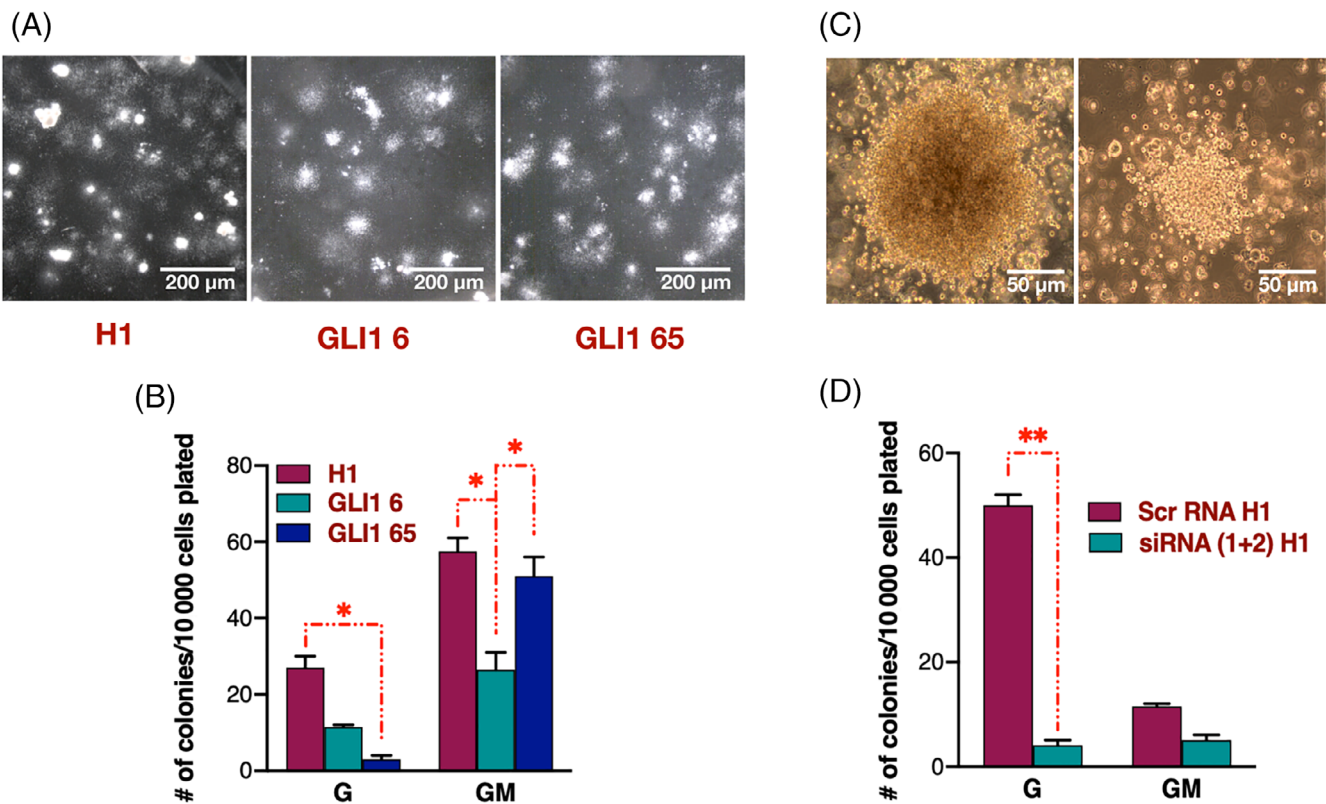


FIGURE 3 Assessment of the effect of GLI1 editing on hematopoietic (mesodermal) differentiation potential of hESCs. A, Representative phase contrast images showing myeloid colonies growing in semisolid media. B, A graph demonstrating the number of myeloid colonies generated from WT H1 hESCs and GLI1-edited cells (GLI1 6 and GLI1 65). Bars represent mean \pm SEM from three independent experiments. G, granulocyte colony forming unit; GM, granulocyte macrophage colony forming unit ($*P < .05$). C, Representative phase contrast images showing granulocyte colonies growing in semisolid media after the siRNA treatment. D, A graph demonstrating the number of myeloid colonies generated from WT H1 hESCs treated with scrambled siRNA and WT H1 hESCs treated with siRNA combination (1 + 2). Bars represent mean \pm SEM from three independent experiments. G, granulocyte colony forming unit; GM, granulocyte macrophage colony forming unit ($*P < .05$). hESCs, human embryonic stem cells; siRNA, small interfering RNA; WT, wild-type

(3 μM).³³ To assess the differentiation dynamic, we evaluated the samples at day 3 by real-time PCR and at day 5 by RNA-Seq. As with our spontaneous differentiation result, real-time PCR and RNA-Seq data demonstrated a significant downregulation of GATA-6 in GLI1-edited cells compared to WT H1 hESCs (Figure 5A). From the volcano plot and pathway analysis (Figures 5B and S7), we observed that SOX17 (P value = 2.12×10^{-12} , FC = -1.57), SOX7 (1.94×10^{-33} , -2.27), and GATA-2 (6.32×10^{-22} , -1.15) were expressed at a significantly lower level in homozygous GLI1-edited cells compared to WT H1 hESCs (Figure 5C).

3.3.6 | Neural differentiation of GLI1 clones (ectodermal lineage)

The effects of GLI1 downregulation on ectodermal differentiation were assessed using PSC neural induction medium. On day 7 of differentiation, neural progenitor cells (NPCs) were collected and assessed using real-time PCR. Half of the cells were transferred to NPC culture media

and propagated for four passages. To assess the morphological properties of NPCs, we cultured them as neurospheres. The results showed that the homozygous GLI1-edited cells have a reduced ability to form neurospheres, as indicated by their smaller size and number (Figure 5D).

Our real-time PCR analysis revealed that during the initial stages of differentiation, at day 7, there was a significant difference in PAX6 and SOX1 expression. Both genes were downregulated in GLI1-edited cells (Figure 5E), while NCAM1 was significantly upregulated (Figure S8). At day 28 of NPC culture, the volcano plot (Figure 5F) and pathway analysis (Figure S8) showed a significant downregulation of NES (1.13×10^{-4} , FC = -0.88), VIM (2.48×10^{-5} , -0.47), and NEFM (1.19×10^{-9} , -1.02) (Figure 5G). This suggested that GLI1 editing inhibited the expression of early neural genes.

To verify whether these early phenotypic differences had an adverse effect on the maturation potential of NPCs derived from homozygous GLI1-edited cells, we conducted spontaneous terminal neural differentiation. Immunofluorescent (IF) staining showed that homozygous NPCs differentiated to neurons and glial cells, as indicated by positive MAP2 and GFAP expression (Figure 5H).

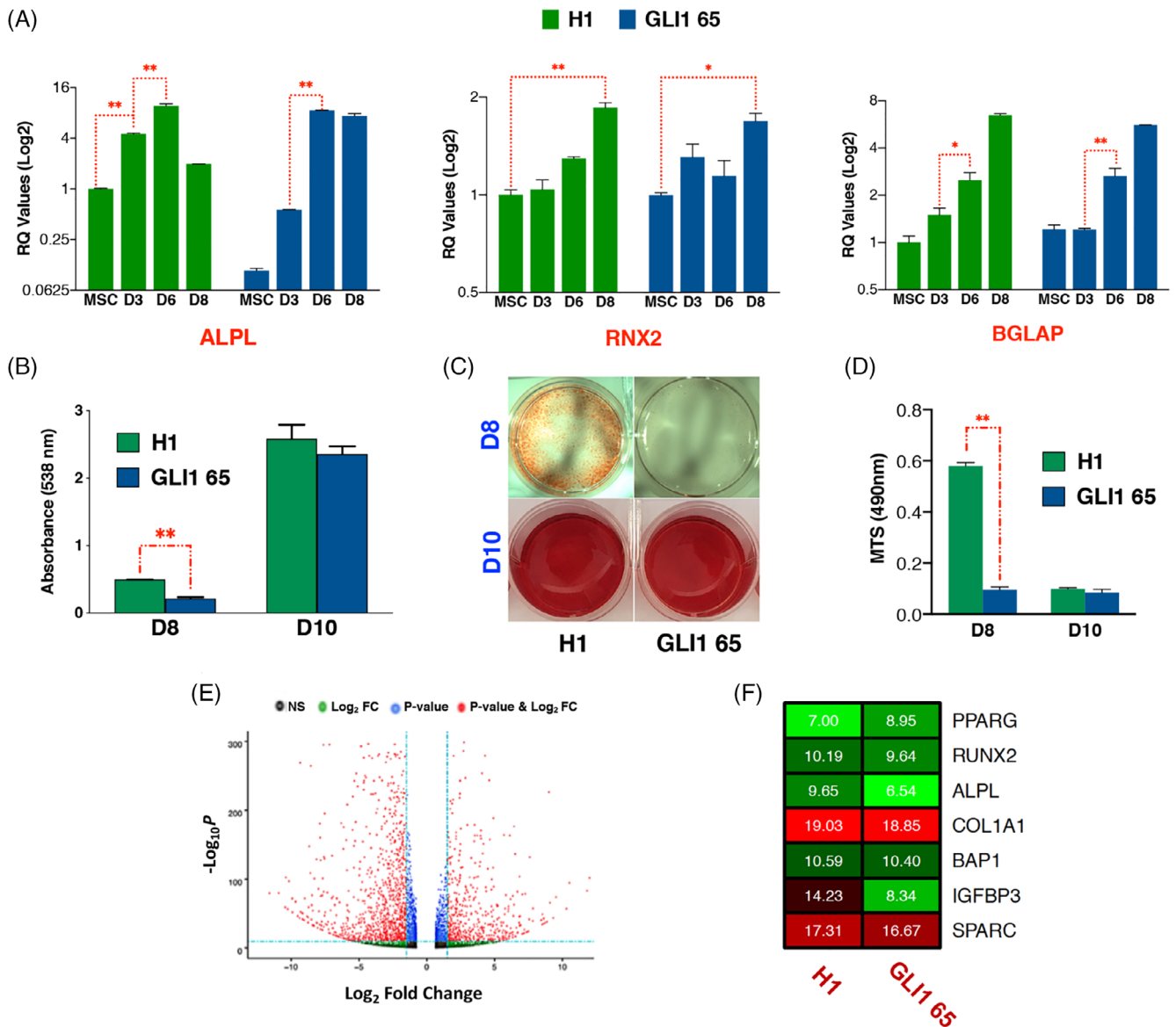


FIGURE 4 Assessment of the effect of GLI1 editing on osteogenic (mesodermal) differentiation potential of hESCs. A, Time course of gene expression in WT H1 hESCs and the GLI1 homozygous-edited cells (GLI1 65) during osteogenic differentiation as determined by real-time PCR. Average expression was normalized to GAPDH, shown as mean \pm SEM from at least three independent experiments ([ALPL, ** $P < .0001$], [RNX2, * $P = .0019$, ** $P = .004$], [BGLAP, * $P = .0138$, ** $P = .0015$]). B,C, A graph and representative images showing that GLI1 homozygous-edited cells had a significant delay in mineralization at day 8 (D8) of osteogenic differentiation (** $P = .000007$). By day 10 (D10), there was no significant difference. D, A graph of the MTS assay showing a significant difference in cell viability between WT H1 hESCs and GLI1-edited cells during osteogenic differentiation (** $P < .0001$). E, Volcano plot showing the statistical significance of RNA-Seq data of osteogenic differentiation. F, Heatmap showing osteogenic gene expression comparison between WT H1 hESCs and GLI1-edited cells. The expression, P value, and fold change data for all gene tables were obtained from RNA-Seq analysis. hESCs, human embryonic stem cells; RNA-Seq, RNA sequencing; siRNA, small interfering RNA; WT, wild-type

3.4 | Spontaneous differentiation in the presence of GANT-61

GANT-61 was found to interfere with GLI1 and GLI2 activity by inhibiting the binding of GLI1 and GLI2 transcription factors to DNA.⁴⁶ GANT-61 does not bind DNA, but rather, it binds to GLI1 (a 5-zinc finger protein) between zinc fingers 2 and 3 at sites E119 and E167.⁴⁷ In light of this, we evaluated the effects of GANT-61 on differentiation using our stem cell model.

First, to validate the effect of GANT-61 inhibition on GLI1 target genes, we performed rt-PCR on GANT-61 treated Rh18 and Rh41 cells. These cell lines express GLI1. We observed significant downregulation of Bcl-2 promoter expression, which is activated in response to GLI1 signaling, in both Rh18 and Rh41 cells (Figure S9).

Next, we evaluated the effect of GANT-61 on GLI1 and SHH pathway members PTCH1 and SMO as well as pluripotency marker expression in hESCs. There were no significant differences in

expression of these markers following 6 or 12 days of GANT-61 treatment (Figure 6A).

Following this, we evaluated the effect of GANT-61 exposure during spontaneous differentiation. After 10 days of differentiation in the presence of GANT-61 treatment, mesodermal and endodermal

gene expression significantly increased, while ectodermal gene expression decreased. After 20 days of exposure, GANT-61 significantly decreased endodermal and mesodermal marker expression (Figure 6B). These effects were similar to those we achieved with the GLI1-edited clones. Additionally, GLI1 and its target PTCH1 were

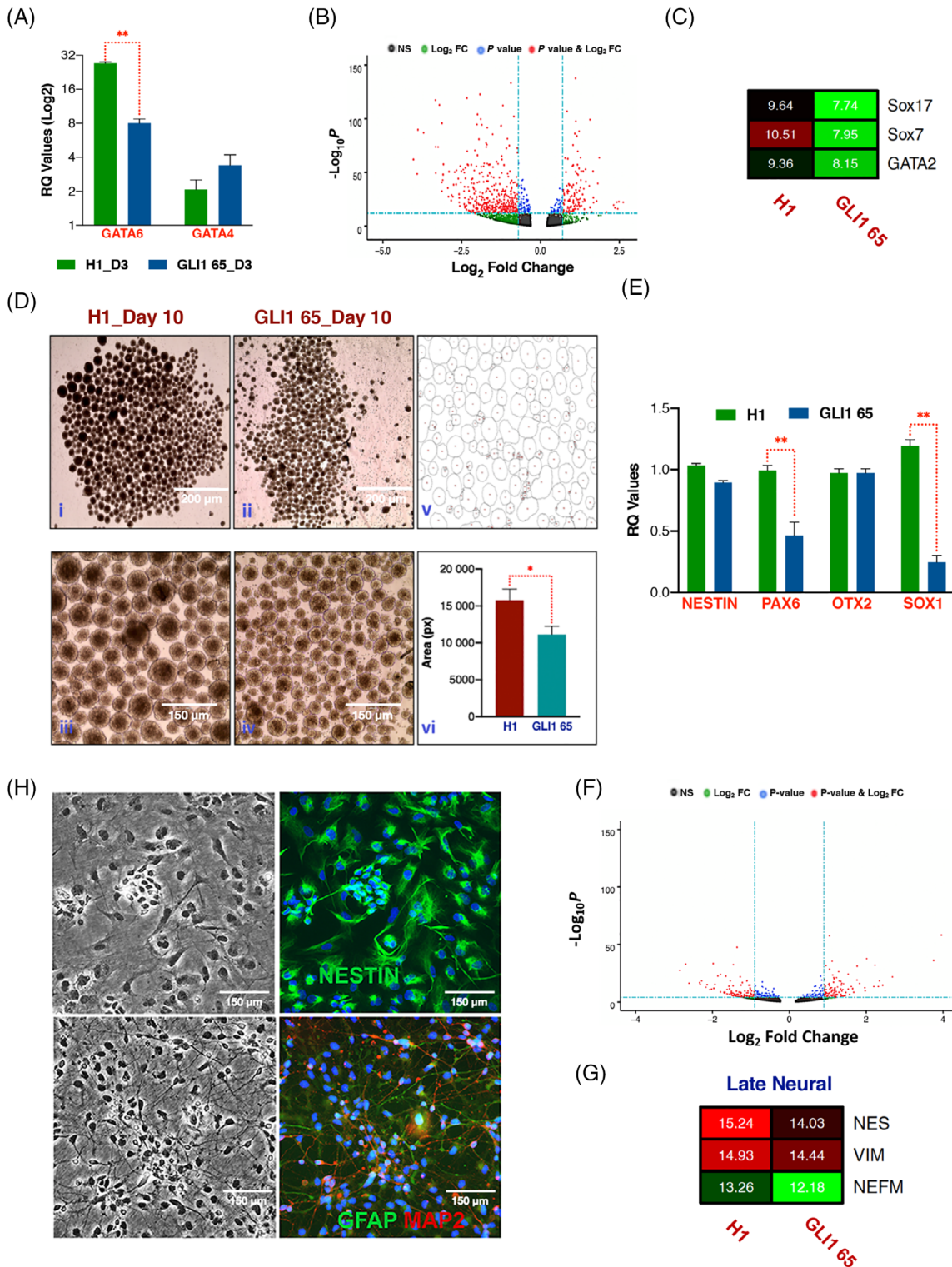


FIGURE 5 Legend on next page.

significantly downregulated during the differentiation process (Figure 6B).

4 | DISCUSSION

GLI1 expression is associated with about a third of human cancers. Its positive feedback loop with GLI2, normally quenched by PTCH1, can drive cancer growth and decrease cancer cell apoptosis.^{9,20} In our previous work, we have shown that developing a greater understanding of the regulatory region in the first intron of the GLI1 gene may provide critical insight into the mechanisms governing this feedback loop. The first intron not only contains highly conserved binding domains, but also acts as a transcriptional enhancer when stimulated by GLI transcription factors and is important in controlling cell proliferation, apoptosis, and differentiation.²³

Based on these findings, we developed a human stem cell model to study the effects of GLI1 expression during the earliest stages of human development. This was achieved by precise editing of a complex enhancer in the first intron of the human GLI1 gene.²³ The result was a deletion of six highly conserved GBS and downregulation of GLI1 expression. Our data show that significant reduction in GLI1 expression occurs in the heterozygous-edited state, and that GLI1 expression is essentially eliminated when both alleles of the region are mutated (homozygous state). This strongly supports the notion that this region is responsible for the positive feedback on GLI1 expression by GLI1 and GLI2.²³ Furthermore, elimination of this intronic region also significantly affects stem cell differentiation toward all three embryonic lineages. Our data demonstrated that GLI1 editing did not affect pluripotency marker expression, but it did inhibit mesodermal and endodermal commitment as well as caused a significant gene dysregulation during neural (ectodermal) differentiation.

With regard to mesodermal commitment, a recent differential gene analysis of GLI1/GLI2 binding regions identified blood vessel development as one of the most upregulated biological processes.¹⁵ To build upon this, our results provide further insight into how extensively GLI1 editing impacts vasculogenesis. During early stages of hemato-endothelial (mesodermal) differentiation, the GLI1-edited cells were skewed toward mesenchymal rather than endothelial and

primitive blood progenitors. At later stages, formation of endothelium was significantly inhibited. Furthermore, expression of RUNX1, an endothelial marker with elevated expression levels in emergent hematopoietic progenitor cells⁴⁸ and during definitive hematopoiesis^{49,50} was significantly downregulated in GLI-edited clones.

To complement these results, the number of CFU-G was also significantly decreased in edited clones, and a similar result was noted after treating WT H1 hESCs with a combination of siRNAs aimed at GLI1 downregulation. We observed this phenomenon in human cells, but interestingly, it also occurred in a GLI1^{null} mouse model, which exhibited decreased response to granulocyte colony stimulating factor (G-CSF) in vivo and decreased myeloid development potential in vitro.⁴²

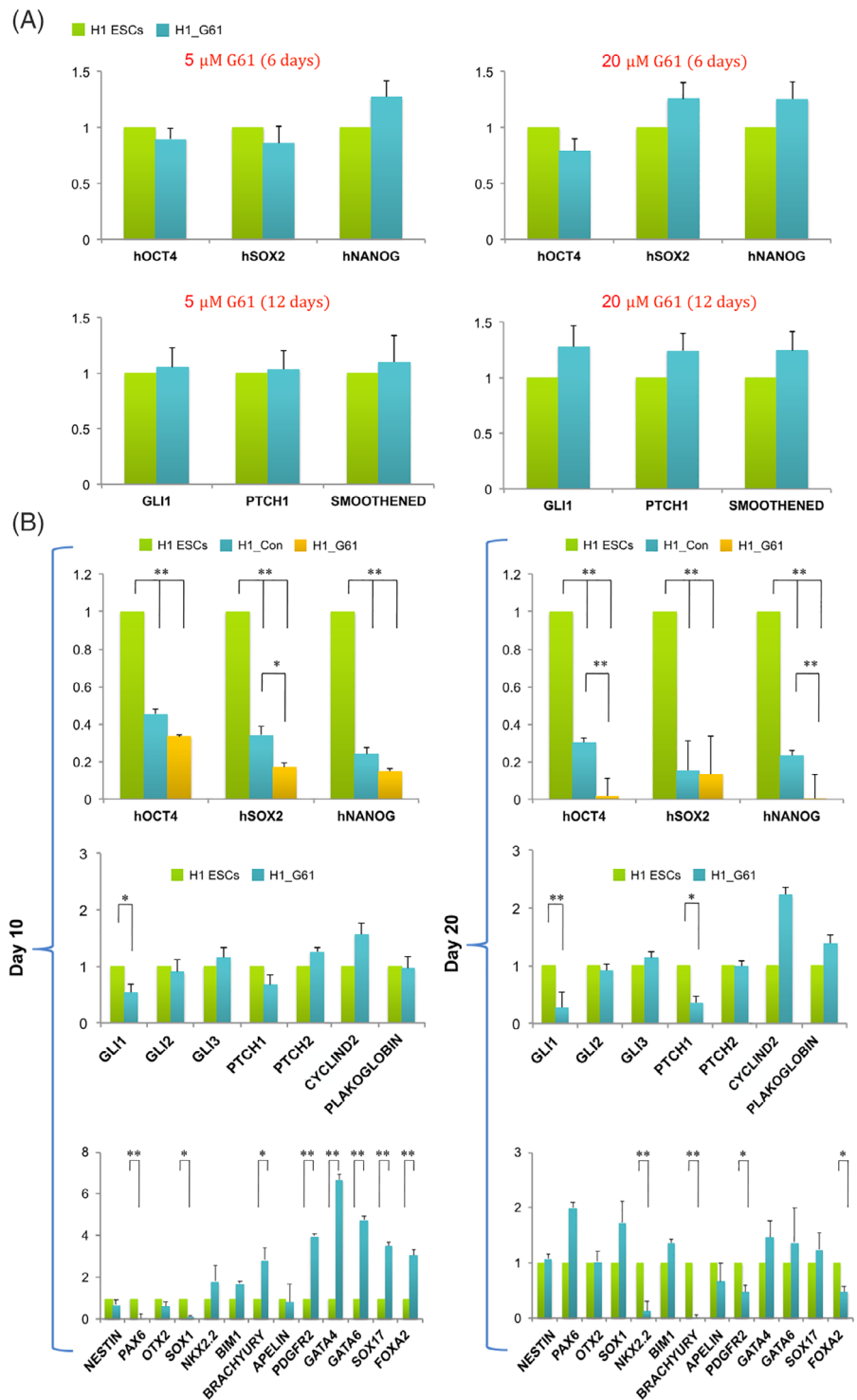
GANT-61 treatments lend further support to this data. GANT-61, which interferes with GLI1 binding, inhibited mesodermal commitment of WT H1 hESCs, in embryoid bodies. This aligns with the significantly reduced mesodermal commitment that GLI1-edited cells exhibit. Thus, it is reasonable to suggest that GANT-61 is potentially inhibiting tumor growth via apoptotic induction coupled with antiangiogenic effects.

Angiogenesis is critical to tissue growth and plays important roles in the pathogenesis of diseases such as cancer. Hypoxia is a key stimulus of angiogenesis and is mediated by HIF-1 α and the oxytocin receptor. GANT-58 (GLI1 inhibitor closely related to GANT-61) has been shown to abrogate oxytocin-induced HIF-1 α expression leading to reduction in angiogenic capacity of human umbilical vein endothelial cells (HUVEC) cells.⁵¹ SHH signaling is known to promote vasculogenesis and angiogenesis,⁵² so downregulating this pathway via GLI1 inhibition is expected to suppress angiogenesis. GANT-61, in addition to its apoptotic and antiangiogenic effects, also reduces stem cell markers in cancer cells.⁵³ Furthermore, SHH/GLI inhibitors other than GANT-61 also suppress tumor angiogenesis and tumor growth in xenograft models.⁵⁴

With regard to osteogenesis, studies in mice demonstrated that GLI1 can induce early osteoblast differentiation during bone formation.⁴³ Furthermore, GLI1 regulates mature bone metabolism by promoting osteoblast differentiation and repressing osteoblast maturation toward osteocytes.⁵⁵ Our data and pathway analysis showed a significant delay in osteoblast differentiation with GLI1

FIGURE 5 Assessment of the effect of GLI1 editing on endodermal and ectodermal differentiation potential of hESCs. A, Real-time PCR analysis of the GLI1 homozygous-edited cells (GLI1 65) showed dramatically reduced expression of GATA-6 during endodermal differentiation as compared to WT H1 hESCs on day 3 (D3) of differentiation (** $P < .0001$). B, Volcano plot showing the statistical significance of RNA-Seq data at day 5 of endodermal differentiation. The expression, P value, and fold change data for all gene tables were obtained from RNA-Seq analysis. C, Heatmap showing endodermal gene expression comparison between WT H1 hESCs and GLI1-edited cells. D, Representative images of neurospheres formed by the WT H1 NPCs (i, iii) and representative images of neurospheres formed by the NPCs from GLI1-edited cells (ii, iv). Representative image showing neurosphere outlines for quantitation, prior to area calculations, performed via the ImageJ program (v). Graphical depiction of average area (reported in pixels) covered by H1 and GLI1-edited neurospheres (vi). The results were from eight experimental trials and reported as \pm SEM ($*P = .030$). E, Real-time PCR analysis showing that editing the first intron of the GLI1 gene in hESCs dramatically reduced the expression of neural markers during day 7 of neural differentiation (** $P < .0001$). F, Volcano plot showing the statistical significance of RNA-Seq data of neural differentiation. G, Heatmap showing neural gene expression comparison between WT H1 hESCs and GLI1 homozygous-edited cells during day 28 of neural differentiation. H, Representative phase contrast and immunofluorescent images showing positive expression of early neural marker Nestin and late neural markers GFAP (green) and MAP2 (red) in GLI1 homozygous-edited cells. hESCs, human embryonic stem cells; NPCs, neural progenitor cells; RNA-Seq, RNA sequencing; WT, wild-type

FIGURE 6 Assessment of the effect of GANT-61 differentiation of hESCs. A, Expression of pluripotency markers, GLI1, PTCH1, and Smoothed (SMO) following 5 and 20 μ M GANT-61 treatment of hESCs maintained in mTeSR1 media. There were no significant differences in marker expression after 6 and 12 days following GANT-61 addition to mTeSR1. B, In the early stage of spontaneous differentiation in embryoid bodies (day 10), GANT-61 treatment downregulated GLI1. Ectodermal differentiation was also inhibited. On the other hand, GANT-61 treatment promoted mesodermal and endodermal differentiation in H1 hESCs. At a later stage (day 20), GANT-61 treatment continued to downregulate the expression of GLI1 and PTCH1 as well as significantly reduced mesodermal and endodermal differentiation markers. hESCs, human embryonic stem cells



editing. Notably, while there was no significant difference in mesenchymal and endothelial cell survival during differentiation, the viability of MSCs differentiating toward osteocytes was significantly reduced.

Additionally, we observed a significant downregulation in genes of endodermal lineage during spontaneous and directed differentiation of GLI1-edited cells compared to WT control. Interestingly, the GLI inhibitor GANT-61 has been found to be successful in treating cancers originating in cells of endodermal lineage. For example, researchers

observed extensive cell death in a panel of seven human colon carcinoma cell lines using GANT-61.⁴⁷ GANT-61 was also found to be an effective inhibitor in the cancer initiating phenotype observed in lung adenocarcinoma cell lines, although issues of bioavailability and toxicity have yet to be addressed.⁵⁶

From an ectodermal perspective, in mice, it was shown that even though elevated GLI1 expression leads to cell cycle arrest and apoptosis in neonatal NSCs, normal expression of GLI1 is necessary for their

self-renewal.⁵⁷ Studies on hESCs revealed that GLI1 was found to be a determinant of ventral floor plate specification and mesencephalic dopamine neuron generation during development.⁵⁸ Our hESC model showed that, during the initiation of spontaneous and directed differentiation, neural differentiation markers PAX6 and SOX1 were expressed at lower levels with homozygous editing than in WT H1 hESCs. Later stages of neural differentiation demonstrated reduction in NES, VIM, and NEFM expression. Furthermore, the edited cells had a reduced ability to form neurospheres. Overall, these data indicate that GLI1-editing delays early neural differentiation.

Our results also revealed statistically significant alteration in GLI1 target gene expression, which impacts cell proliferation (HHIP, IGFBP6, MYCN, CCND2) and cell differentiation (SSP1). The HHIP gene is upstream of the SHH pathway. Its downstream targets IGFBP6, MYCN, and CCND2 are transcriptionally upregulated, thereby increasing cellular proliferative potential. Regarding the SPP1 gene, it is downstream of both SHH and BMP pathways. SPP1 is transcriptionally activated by GLI1 to induce osteogenic differentiation. In our GLI1-edited cells, the expression levels of these target genes were significantly downregulated (Figure S10).

In totality, this work centers around the foundational concept that transcriptional regulation occurs in a landscape of protein complexes that modulate the expression of genes. Key regulatory events occur in discrete areas that can coordinate the expression of dozens of genes and together, with spatial control of enhancers, orchestrate normal development. Alterations of regulatory regions are associated with disease burdens. In the case of GLI1, the first intron represents such a region. Public data reveal dozens of transcription factors that bind to this region, and we have demonstrated that such binding along with BRD4, H2A.z, and histone marks can account for much of the activity of the GLI1 positive feedback loop.²³

5 | SUMMARY

Our stem cell model, based on the editing of a regulatory region in the first intron of GLI1, highlights the importance of the six GBS in this region during stem cell differentiation and tissue development. RNA-Seq data and pathway analyses clearly show that GLI1 is highly involved in regulating stem cell differentiation toward all three embryonic lineages and plays a crucial role in vasculogenesis and hematopoiesis. These data suggest that manipulating this region can modulate GLI1 expression, which highlights the possibility for new therapeutic strategies that are focused on targeting the positive GLI feedback loop in order to treat human malignancies.

ACKNOWLEDGMENTS

We would like to acknowledge the contribution of NUSeq Core: Center for Genetic Medicine (Feinberg School of Medicine - Northwestern University). This work was supported in part by the Eisenberg Foundation for Charities (P. M. I.) and by P01ES010549 from the NIH (P. M. I., D. O. W.).

CONFLICT OF INTEREST

The authors declared no potential conflicts of interest.

AUTHOR CONTRIBUTIONS

Y.G.: study conception and design, collection of data, bioinformatic analysis, ESC differentiation, data assembly and interpretation, manuscript writing, final approval of manuscript; H.G.: study conception and design, collection of data, ESC differentiation, final approval of manuscript; M.P.: bioinformatic analysis, data assembly and interpretation, manuscript writing, final approval of manuscript; R.T., J.W.Y.: study conception and design, collection of data, final approval of manuscript; I.P.B.: siRNA design, final approval of manuscript; X.A.G.: siRNA design, siRNA production, final approval of manuscript; X.-N.L.: contributed analysis tools, final approval of manuscript; D.O.W., P.M.I.: study conception and design, data assembly and interpretation, final approval of manuscript; V.G.: study conception and design, collection of data, ESC differentiation, data assembly and interpretation, final approval of manuscript.

DATA AVAILABILITY STATEMENT

The data that support the findings of this study are available from the corresponding author upon reasonable request.

ORCID

Mariana Perepitchka  <https://orcid.org/0000-0002-3565-6670>

REFERENCES

- Hui CC, Angers S. Gli proteins in development and disease. *Annu Rev Cell Dev Biol.* 2011;27:513-537.
- Robbins DJ, Fei DL, Riobo NA. The hedgehog signal transduction network. *Sci Signal.* 2012;5:re6.
- Villavicencio EH, Walterhouse DO, Iannaccone PM. The sonic hedgehog-patched-gli pathway in human development and disease. *Am J Hum Genet.* 2000;67:1047-1054.
- Walterhouse DO, Lamm ML, Villavicencio E, Iannaccone PM. Emerging roles for hedgehog-patched-gli signal transduction in reproduction. *Biol Reprod.* 2003;69:8-14.
- Palencia-Campos A, Ullah A, Nevado J, et al. GLI1 inactivation is associated with developmental phenotypes overlapping with Ellis-van Creveld syndrome. *Hum Mol Genet.* 2017;26:4556-4571.
- Walterhouse DO, Yoon JW, Iannaccone PM. Developmental pathways: sonic hedgehog-patched-GLI. *Environ Health Perspect.* 1999; 107:167-171.
- Iannaccone PM et al. The hedgehog signaling pathway in development and disease. In: Epstein CJ, Erickson RP, Wynshaw-Boris A, et al., *Inborn Errors of Development: The Molecular Basis of Clinical Disorders of Morphogenesis*; 2nd eds. Oxford: Oxford University Press; 2008:263-280.
- Yu M, Gipp J, Yoon JW, Iannaccone P, Walterhouse D, Bushman W. Sonic hedgehog-responsive genes in the fetal prostate. *J Biol Chem.* 2009;284:5620-5629.
- Yoon JW, Gilbertson R, Iannaccone S, Iannaccone P, Walterhouse D. Defining a role for Sonic hedgehog pathway activation in desmoplastic medulloblastoma by identifying GLI1 target genes. *Int J Cancer.* 2009;124:109-119.
- Lamm ML, Catbagan WS, Laciak RJ, et al. Sonic hedgehog activates mesenchymal Gli1 expression during prostate ductal bud formation. *Dev Biol.* 2002;249:349-366.
- High A, Zedan W. Basal cell nevus syndrome. *Curr Opin Oncol.* 2005; 17:160-166.

12. Regl G, Neill GW, Eichberger T, et al. Human GLI2 and GLI1 are part of a positive feedback mechanism in Basal Cell Carcinoma. *Oncogene*. 2002;21:5529-5539.
13. Yoon JW, Kita Y, Frank DJ, et al. Gene expression profiling leads to identification of GLI1-binding elements in target genes and a role for multiple downstream pathways in GLI1-induced cell transformation. *J Biol Chem*. 2002;277:5548-5555.
14. Carpenter RL, Paw I, Zhu H, et al. The gain-of-function GLI1 transcription factor TGLI1 enhances expression of VEGF-C and TEM7 to promote glioblastoma angiogenesis. *Oncotarget*. 2015;6:22653-22665.
15. Ali SA, Niu B, Cheah KSE, Alman B. Unique and overlapping GLI1 and GLI2 transcriptional targets in neoplastic chondrocytes. *PLoS One*. 2019;14:e0211333.
16. Xu X, Liu H, Zhang H, et al. Sonic hedgehog-GLI family zinc finger 1 signaling pathway promotes the growth and migration of pancreatic cancer cells by regulating the transcription of eukaryotic translation initiation factor 5A2. *Pancreas*. 2015;44:1252-1258.
17. Ghanbari A, Cheraghzadeh Z, Mahmoudi R, Zibara K, Hosseini E. GLI inhibitors overcome Erlotinib resistance in human pancreatic cancer cells by modulating E-cadherin. *J Chemother*. 2019;31:141-149.
18. Yoon JW, Lamm M, Chandler C, Iannaccone P, Walterhouse D. Up-regulation of GLI1 in vincristine-resistant rhabdomyosarcoma and Ewing sarcoma. *BMC Cancer*. 2020;20:511.
19. Gu D, Xie J. Non-canonical Hh signaling in cancer-current understanding and future directions. *Cancers*. 2015;7:1684-1698.
20. Yoon JW, Gallant M, Lamm MLG, et al. Noncanonical regulation of the Hedgehog mediator GLI1 by c-MYC in Burkitt lymphoma. *Mol Cancer Res*. 2013;11:604-615.
21. Yuan X, Cao J, He X, et al. Ciliary IFT80 balances canonical versus non-canonical hedgehog signalling for osteoblast differentiation. *Nat Commun*. 2016;7:11024.
22. Zwerner JP, Joo J, Warner KL, et al. The EWS/FLI1 oncogenic transcription factor deregulates GLI1. *Oncogene*. 2008;27:3282-3291.
23. Taylor R, Long J, Yoon JW, et al. Regulation of GLI1 by cis DNA elements and epigenetic marks. *DNA Repair*. 2019;79:10-21.
24. Chen Q, Shou P, Zheng C, et al. Fate decision of mesenchymal stem cells: adipocytes or osteoblasts? *Cell Death Differ*. 2016;23:1128-1139.
25. Ahmed S, Gan HT, Lam CS, et al. Transcription factors and neural stem cell self-renewal, growth and differentiation. *Cell Adh Migr*. 2009;3:412-424.
26. Wu SM, Choo AB, Yap MG, Chan KK. Role of Sonic hedgehog signaling and the expression of its components in human embryonic stem cells. *Stem Cell Res*. 2010;4:38-49.
27. Po A, Ferretti E, Miele E, et al. Hedgehog controls neural stem cells through p53-independent regulation of Nanog. *EMBO J*. 2010;29:2646-2658.
28. Yoon JW, Lamm M, Iannaccone S, et al. p53 modulates the activity of the GLI1 oncogene through interactions with the shared coactivator TAF9. *DNA Repair*. 2015;34:9-17.
29. Bai CB, Auerbach W, Lee JS, Stephen D, Joyner AL. Gli2, but not Gli1, is required for initial Shh signaling and ectopic activation of the Shh pathway. *Development*. 2002;129:4753-4761.
30. Drakopoulou E, Outram SV, Rowbotham NJ, et al. Non-redundant role for the transcription factor Gli1 at multiple stages of thymocyte development. *Cell Cycle*. 2010;9:4144-4152.
31. Park HL, Bai C, Platt KA, et al. Mouse Gli1 mutants are viable but have defects in SHH signaling in combination with a Gli2 mutation. *Development*. 2000;127:1593-1605.
32. Thomson JA, Itskovitz-Eldor J, Shapiro SS, et al. Embryonic stem cell lines derived from human blastocysts. *Science*. 1998;282:1145-1147.
33. Siller R, Sullivan GJ. Rapid screening of the endodermal differentiation potential of human pluripotent stem cells. *Curr Protoc Stem Cell Biol*. 2017;43:1G.7.1-1G.7.23.
34. Lian X, Bao X, al-Ahmad A, et al. Efficient differentiation of human pluripotent stem cells to endothelial progenitors via small-molecule activation of WNT signaling. *Stem Cell Reports*. 2014;3:804-816.
35. Choi KD, Vodyanik M, Slukvin II. Hematopoietic differentiation and production of mature myeloid cells from human pluripotent stem cells. *Nat Protoc*. 2011;6:296-313.
36. Yun C, Weiner JA, Chun DS, et al. Mechanistic insight into the effects of Aryl Hydrocarbon Receptor activation on osteogenic differentiation. *Bone Rep*. 2017;6:51-59.
37. Galat Y, Dambaeva S, Elcheva I, et al. Cytokine-free directed differentiation of human pluripotent stem cells efficiently produces hemogenic endothelium with lymphoid potential. *Stem Cell Res Ther*. 2017;8:67.
38. Li Y, Zhang Q, Tian R, et al. Lysosomal transmembrane protein LAP-TM4B promotes autophagy and tolerance to metabolic stress in cancer cells. *Cancer Res*. 2011;71:7481-7489.
39. Beauchamp E, Bulut G, Abaan O, et al. GLI1 is a direct transcriptional target of EWS-FLI1 oncoprotein. *J Biol Chem*. 2009;284:9074-9082.
40. Campbell VT, Nadesan P, Ali SA, et al. Hedgehog pathway inhibition in chondrosarcoma using the smoothed inhibitor IPI-926 directly inhibits sarcoma cell growth. *Mol Cancer Ther*. 2014;13:1259-1269.
41. Houde C, Li Y, Song L, et al. Overexpression of the NOTCH ligand JAG2 in malignant plasma cells from multiple myeloma patients and cell lines. *Blood*. 2004;104:3697-3704.
42. Merchant A, Joseph G, Wang Q, Brennan S, Matsui W. Gli1 regulates the proliferation and differentiation of HSCs and myeloid progenitors. *Blood*. 2010;115:2391-2396.
43. Hojo H, Ohba S, Yano F, et al. Gli1 protein participates in Hedgehog-mediated specification of osteoblast lineage during endochondral ossification. *J Biol Chem*. 2012;287:17860-17869.
44. Shi Y, He G, Lee WC, McKenzie JA, Silva MJ, Long F. Gli1 identifies osteogenic progenitors for bone formation and fracture repair. *Nat Commun*. 2017;8:2043.
45. Galat Y, Galat Y, Perepitchka M, Jennings LJ, Iannaccone PM, Hendrix MJC. Transgene reactivation in induced pluripotent stem cell derivatives and reversion to pluripotency of induced pluripotent stem cell-derived mesenchymal stem cells. *Stem Cells Dev*. 2016;25:1060-1072.
46. Lauth M, Bergstrom A, Shimokawa T, Toftgard R. Inhibition of GLI-mediated transcription and tumor cell growth by small-molecule antagonists. *Proc Natl Acad Sci USA*. 2007;104:8455-8460.
47. Agyeman A, Jha BK, Mazumdar T, Houghton JA. Mode and specificity of binding of the small molecule GANT61 to GLI determines inhibition of GLI-DNA binding. *Oncotarget*. 2014;5:4492-4503.
48. North T, Gu TL, Stacy T, et al. Cbfa2 is required for the formation of intra-aortic hematopoietic clusters. *Development*. 1999;126:2563-2575.
49. Sugimura R, Jha DK, Han A, et al. Haematopoietic stem and progenitor cells from human pluripotent stem cells. *Nature*. 2017;545:432-438.
50. Galat Y, Elcheva I, Dambaeva S, et al. Application of small molecule CHIR99021 leads to the loss of hemangioblast progenitor and increased hematopoiesis of human pluripotent stem cells. *Exp Hematol*. 2018;65:38-48.
51. Zhu J, Wang H, Zhang X, Xie Y. Regulation of angiogenic behaviors by oxytocin receptor through Gli1-induced transcription of HIF-1alpha in human umbilical vein endothelial cells. *Biomed Pharmacother*. 2017;90:928-934.
52. Byrd N, Gabel L. Hedgehog signaling in murine vasculogenesis and angiogenesis. *Trends Cardiovasc Med*. 2004;14:308-313.
53. Po A, Silvano M, Miele E, et al. Noncanonical GLI1 signaling promotes stemness features and in vivo growth in lung adenocarcinoma. *Oncogene*. 2017;36:4641-4652.
54. Lei X, Zhong Y, Huang L, et al. Identification of a novel tumor angiogenesis inhibitor targeting Shh/Gli1 signaling pathway in non-small cell lung cancer. *Cell Death Dis*. 2020;11:232.

55. Kitaura Y, Hojo H, Komiyama Y, Takato T, Chung UI, Ohba S. Gli1 haploinsufficiency leads to decreased bone mass with an uncoupling of bone metabolism in adult mice. *PLoS One*. 2014;9:e109597.
56. Dimou A, Bamias A, Gogas H, Syrigos K. Inhibition of the Hedgehog pathway in lung cancer. *Lung Cancer*. 2019;133:56-61.
57. Galvin KE, Ye H, Erstad DJ, Feddersen R, Wetmore C. Gli1 induces G2/M arrest and apoptosis in hippocampal but not tumor-derived neural stem cells. *STEM CELLS*. 2008;26:1027-1036.
58. Denham M, Thompson LH, Leung J, Pébay A, Björklund A, Dottori M. Gli1 is an inducing factor in generating floor plate progenitor cells from human embryonic stem cells. *STEM CELLS*. 2010;28:1805-1815.

SUPPORTING INFORMATION

Additional supporting information may be found online in the Supporting Information section at the end of this article.

How to cite this article: Galat Y, Gu H, Perepitchka M, et al. CRISPR editing of the GLI1 first intron abrogates GLI1 expression and differentially alters lineage commitment. *Stem Cells*. 2021;39:564–580. <https://doi.org/10.1002/stem.3341>